Correspondence between phase oscillator network and classical XY model with the same random and frustrated interactions

Tomoyuki Kimoto[1,*] and Tatsuya Uezu[2,†]
[1]*National Institute of Technology, Oita College, Oita 870-0152, Japan*
[2]*Graduate School of Humanities and Sciences, Nara Women's University, Nara 630-8506, Japan*

(Received 26 February 2019; revised manuscript received 19 June 2019; published 16 August 2019)

We study correspondence between a phase oscillator network with distributed natural frequencies and a classical XY model at finite temperatures with the same random and frustrated interactions used in the Sherrington-Kirkpatrick model. We perform numerical calculations of the spin glass order parameter q and the distributions of the local fields $P(R)$, where R is the amplitude of the local field. As a result, we find that the parameter dependences of $P(R)$ in both models agree fairly well in all ranges of parameters in the spin glass phase and those of q agree at least for lower values of parameters in the spin glass phase, if parameters are normalized by using the previously obtained correspondence relation between two models with the same other types of interactions. Furthermore, we numerically calculate the time evolution of quantities such as the instantaneous local field in the phase oscillator network in order to study the roles of synchronous and asynchronous oscillators. We also study the self-consistent equation of the local fields in the oscillator network and XY model derived by the mean-field approximation.

DOI: 10.1103/PhysRevE.100.022213

I. INTRODUCTION

The classical XY model which describes magnetism has been studied and a lot of phase transition phenomena have been found [1]. On the other hand, there are a lot of synchronization phenomena in nature such as circadian rhythms, heartbeats, collective firing of fireflies, and so on [2,3]. For such synchronization phenomena, a phase oscillator model which describes oscillations only by phases has been proposed [4], and the synchronization-desynchronization phase transition point has been analytically obtained in the case of the uniform infinite-range interaction [5]. The models which are described only by phases are not special in the sense that the differential equations for phases are derived when nonlinear differential equations which exhibit limit cycle oscillations are weakly coupled [6]. The phase oscillator model with the uniform infinite-range interaction is called the Kuramoto model. Since Kuramoto proposed the model, there have been many extensions of the model, and many interesting phenomena such as chimera states and the synchronization due to common noises have been found, and attempts to identify a dynamical system from experimental data have been made [7].

In the XY model and the phase oscillator network with the same interaction, the order parameters are the same, and it is trivial that the XY model with zero temperature and the phase oscillator network with uniform natural frequencies are equivalent, but thus far no relations between these two models have been found beyond this. A few years ago, for a class of infinite-range interactions, we found the correspondence between the XY model with nonzero temperature and the phase oscillator network with distributed natural frequencies [8]. Specifically, temperature T in the XY model corresponds to the width of distribution of natural frequencies in the oscillator network, e.g., T corresponds to $\sqrt{2/\pi}\sigma$ where σ is the standard deviation when the distribution is Gaussian. The integration kernels for the saddle point equations (SPEs) for the XY model and the self-consistent equations (SCEs) for the phase oscillator network correspond as well. Furthermore, for several interactions, there exists one-to-one correspondence between solutions for both models, and thus it is found that the critical exponents are the same in both models [9].

When we study models with the interactions for which the correspondence between two models is known to exist, if we derive the SPEs or SCEs, their solutions, and critical exponents for one model, we can obtain those of the other model by using the correspondence between the two models. Also, if we find interesting behaviors in one model, similar kinds of behaviors are expected to be observed in the other model, at least at very low temperature T or standard deviation σ, because the two models are the same at $T = 0$ and $\sigma = 0$. Therefore, it is very interesting and important to clarify interactions for which the correspondence between the two models exists.

So far, it has been found that correspondence holds when a few order parameters exist and their SPEs and SCEs are derived for a class of infinite-range interactions with or without randomness and without frustration. On the other hand, even if interactions are infinite range, if they are random and frustrated, the correspondence between the two models has not yet been clarified. Random and frustrated interactions are very interesting in themselves, because not only is randomness ubiquitous in nature but also nontrivial phenomena such as spin glass phases exist in some models. One such interaction was studied by Sherrington and Kirkpatrick and is

*kimoto@oita-ct.ac.jp
†uezu@cc.nara-wu.ac.jp

called the Sherrington-Kirkpatrick (SK) model [10]. We study this interaction in this paper.

It is well known that the SK model exhibits the spin glass phase for some parameter ranges. In the spin glass phase, the total magnetization is zero, but locally each spin is frozen and has nonzero local magnetization. The spins with continuous n components are also studied in Ref. [10], and the SPEs are derived and the spin glass phase is obtained. On the other hand, for the phase oscillator network, more than two decades ago, a numerical study for the SK interaction was performed by Daido and nontrivial behaviors were obtained [11]. That is, the quasientrainment state was observed, in which the substantial frequency for each oscillator is very small, but phases between two such oscillators diffuse slowly. Furthermore, the distribution of the local fields (LFs) undergoes a phase transition in which the peak position of the distribution changes from zero to nonzero value as a parameter changes and this is called the volcano transition.

In this paper, we perform numerical calculations and study the spin glass order parameter q and distributions of LFs in both models. In addition, in order to study the roles of synchronous and asynchronous oscillators in the phase oscillator network, we numerically calculate the time evolution of quantities such as phases and the local fields, and derive the SCEs of the LFs assuming that only the synchronous oscillators exist. Similarly, in the XY model, by using the naive mean-field approximation, we derive the SCEs of the LFs. We compare theoretical results with numerical ones in both models.

The structure of this paper is as follows. In Sec. II, we formulate the problem and describe the SPEs. In Sec. III, we show the results of numerical simulations. Summary and discussion are given in Sec. IV. In the Appendix, we derive the disorder averaged free energy per spin and the SPEs under the ansatz of the replica symmetry in the XY model.

II. FORMULATION

The classical XY model consists of N XY spins $X_j = (\cos\phi_j, \sin\phi_j)$, $(j = 1, \cdots, N)$, where ϕ_j is the phase of the jth XY spin. The Hamiltonian H is given by

$$H = -\sum_{j<k}^{N} J_{jk}\cos(\phi_j - \phi_k), \tag{1}$$

where J_{jk} is the interaction between the jth and kth XY spins. On the other hand, in the phase oscillator network, each oscillator is described by a phase. Let ϕ_j be the phase of the jth phase oscillator. The evolution equation for ϕ_j is given by

$$\frac{d\phi_j}{dt} = \omega_j + \sum_{k=1}^{N} J_{jk}\sin(\phi_k - \phi_j), \tag{2}$$

where J_{jk} is the interaction from the kth to jth phase oscillators and the constant ω_j is the natural frequency. We assume that ω_j is a random variable generated from the probability density function $g(\omega)$. We assume that $g(\omega)$ is one-humped and symmetric with respect to its center ω_0. In this paper, for $g(\omega)$ we adopt the Gaussian distribution with mean zero and standard deviation σ, $\mathcal{N}(0, \sigma^2)$. We assume both systems have the following SK interaction in common:

$$J_{jk} = \frac{J}{\sqrt{N}} z_{jk}, \tag{3}$$

where z_{jk} is a random variable obeying the Gaussian distribution $\mathcal{N}(0, 1)$. Moreover, we assume $J_{jj} = 0$ and $J_{jk} = J_{kj} (j \neq k)$.

Now, by using the replica method, we derive the SPEs for the XY model, which is originally obtained in Ref. [10].

First, in the XY model, we define the following spin glass order parameter q:

$$q = \mathrm{Max}\left(\left| \frac{1}{N}\sum_{j=1}^{N} e^{i\left(\phi_j^\alpha - \phi_j^\beta\right)} \right|, \left| \frac{1}{N}\sum_{j=1}^{N} e^{i\left(\phi_j^\alpha - \left(-\phi_j^\beta\right)\right)} \right| \right), \tag{4}$$

where $i = \sqrt{-1}$, ϕ_j^α $(1 \leqslant j \leqslant N)$ and ϕ_j^β $(1 \leqslant j \leqslant N)$ are phases of two replicas α and β that have the same interaction $\{J_{jk}\}$. The first argument is calculated by the phase difference between ϕ_j^α and ϕ_j^β, and the second argument is calculated by the phase difference between ϕ_j^α and $-\phi_j^\beta$. Since the Hamiltonian (1) has the reversal symmetry, that is, it is invariant under the reversal of signs of phases $\{\phi_j\} \to \{-\phi_j\}$, we calculate the summation for the reversal phase $-\phi_j^\beta$ shown in the second argument. Since we set $J = 1$, then $q > 0$ when the system is in the spin glass state, and $q = 0$ when it is in the paramagnetic state. This order parameter is exactly the same as that obtained by Sherrington and Kirkpatrick [10]. We derive the SPE for the spin glass order parameter. See the Appendix for details.

Introducing n replicas, we define the following order parameters. For $\alpha < \beta$,

$$q_{\mathrm{cc}}^{\alpha\beta} = \frac{1}{N}\sum_i \cos\phi_i^\alpha \cos\phi_i^\beta,\ q_{\mathrm{ss}}^{\alpha\beta} = \frac{1}{N}\sum_i \sin\phi_i^\alpha \sin\phi_i^\beta, \tag{5}$$

$$q_{\mathrm{cs}}^{\alpha\beta} = \frac{1}{N}\sum_i \cos\phi_i^\alpha \sin\phi_i^\beta,\ q_{\mathrm{sc}}^{\alpha\beta} = \frac{1}{N}\sum_i \sin\phi_i^\alpha \cos\phi_i^\beta, \tag{6}$$

and for $\alpha = 1, \cdots, n$

$$Q_{\mathrm{cc}}^{\alpha} = \frac{1}{N}\sum_i \cos^2\phi_i^\alpha, \quad Q_{\mathrm{ss}}^{\alpha} = \frac{1}{N}\sum_i \sin^2\phi_i^\alpha,$$

$$Q_{\mathrm{cs}}^{\alpha} = \frac{1}{N}\sum_i \cos\phi_i^\alpha \sin\phi_i^\alpha.$$

By using the standard recipe, we obtain the disorder averaged free energy per spin $\bar{f} = -\lim_{N\to\infty}(\beta N)^{-1}\overline{\log Z}$ by the replica method, where $\beta = \frac{1}{k_{\mathrm{B}}T}$, k_{B} is the Boltzmann constant, and Z is the partition function. We set $k_B = 1$. Here, $\overline{\cdots}$ implies the average over $\{J_{ij}\}$. Assuming the replica symmetry, we obtain

$$\bar{f}_{\mathrm{RS}} = -\frac{1}{\beta}\left\{ \frac{\beta^2 J^2}{4}\left(q_{\mathrm{cc}}^2 + q_{\mathrm{ss}}^2 + q_{\mathrm{cs}}^2 + q_{\mathrm{sc}}^2 - Q_{\mathrm{cc}}^2 - Q_{\mathrm{ss}}^2 - 2Q_{\mathrm{cs}}^2\right) + \int Dx \int Dy \log \int d\phi M(\phi|x, y) \right\}, \tag{7}$$

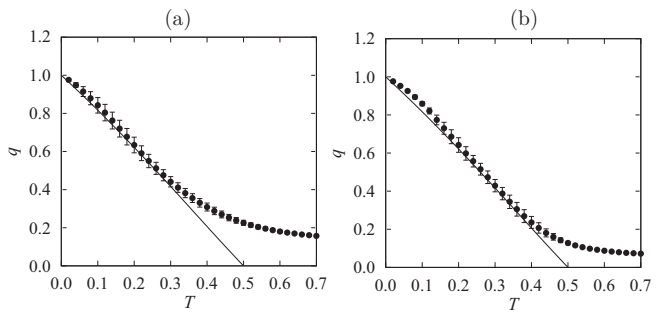

FIG. 1. Temperature dependence of the sample average of q in the XY model. (a) $N = 100$. (b) $N = 500$.

$$
\begin{aligned}
&M(\phi|x,y)\\
&= \exp\Bigg[\frac{\beta^2J^2}{2}(Q_{\rm cc}-q_{\rm cc})\cos^2\phi+\frac{\beta^2J^2}{2}(Q_{\rm ss}-q_{\rm ss})\sin^2\phi\\
&\quad+\beta^2J^2\left(Q_{\rm cs}-\frac{q_{\rm cs}+q_{\rm cs}}{2}\right)\sin\phi\cos\phi\\
&\quad+\beta J\sqrt{\frac{q_{\rm cc}q_{\rm ss}-\left(\frac{q_{\rm cs}+q_{\rm sc}}{2}\right)^2}{q_{\rm ss}}}\cos\phi\,x\\
&\quad+\beta J\left(\frac{q_{\rm cs}+q_{\rm sc}}{2\sqrt{q_{\rm ss}}}\cos\phi+\sqrt{q_{\rm ss}}\sin\phi\right)y\Bigg]. \qquad (8)
\end{aligned}
$$

Here, we assume $q_{\rm ss} > 0, q_{\rm cc} > 0$ and $q_{\rm cc}q_{\rm ss} > (\frac{q_{\rm cs}+q_{\rm sc}}{2})^2$. From this, we obtain the following SPEs:

$$
\begin{aligned}
&Q_{\rm cc} = [\langle\cos^2\phi\rangle], \quad Q_{\rm ss} = [\langle\sin^2\phi\rangle] = 1 - Q_{\rm cc},\\
&Q_{\rm cs} = [\langle\sin\phi\cos\phi\rangle], \qquad (9)
\end{aligned}
$$

$$
\begin{aligned}
&q_{\rm cc} = [\langle\cos\phi\rangle^2],\ q_{\rm ss} = [\langle\sin\phi\rangle^2],\\
&q_{\rm cs} = [\langle\sin\phi\rangle\langle\cos\phi\rangle] = q_{\rm sc}, \qquad (10)
\end{aligned}
$$

$$
[\cdots] \equiv \int Dx \int Dy \cdots,
$$

$$
\langle\cdots\rangle \equiv \frac{\int d\phi M(\phi|x,y)\ \cdots}{\int d\phi M(\phi|x,y)}. \qquad (11)
$$

q defined by Eq. (4) is rewritten by using these quantities as

$$
\begin{aligned}
q = \ &\mathrm{Max}\left\{\sqrt{\left(q_{\rm cc}^{\alpha\beta}+q_{\rm ss}^{\alpha\beta}\right)^2+\left(q_{\rm sc}^{\alpha\beta}-q_{\rm cs}^{\alpha\beta}\right)^2},\right.\\
&\left.\sqrt{\left(q_{\rm cc}^{\alpha\beta}-q_{\rm ss}^{\alpha\beta}\right)^2+\left(q_{\rm sc}^{\alpha\beta}+q_{\rm cs}^{\alpha\beta}\right)^2}\right\}. \qquad (12)
\end{aligned}
$$

The Hamiltonian is invariant under the coordinate transformations $\phi_j' = \phi_j + \phi_0$ with a constant ϕ_0 for all j, and, under the reversal of coordinates, $\phi_j' = -\phi_j$ for all j. q is invariant under these transformations. By $\phi_j' = \pi/2 - \phi_j$, $\cos\phi_j$ and $\sin\phi_j$ are interchanged. We also make variable transformations $x' = y,\ y' = x$. We require that $M(\phi|x,y)$ and $M(\phi'|y,x)$ are the same functional form since $\bar{f}_{\rm RS}$ should be invariant under coordinate transformations. Then, we obtain

$$
\begin{aligned}
&Q_{\rm cc} - q_{\rm cc} = Q_{\rm ss} - q_{\rm ss},\ \sqrt{\frac{q_{\rm cc}q_{\rm ss}-q_{\rm cs}^2}{q_{\rm ss}}} = \sqrt{q_{\rm ss}},\\
&q_{\rm cs} = 0. \qquad (13)
\end{aligned}
$$

Thus, we obtain $Q_{\rm cc} = Q_{\rm ss} = \frac{1}{2}, q_{\rm cc} = q_{\rm ss}, q_{\rm sc} = 0$. By $\phi_j' = -\phi_j$, $\sin\phi_j\cos\phi_j$ changes its sign, and we require that $M(\phi|x,y)$ and $M(\phi'|x,-y)$ are the same functional form, and then $Q_{\rm cs} = 0$ follows. By the Markov chain Monte Carlo simulations, we observe that $Q_{\rm cc} \simeq Q_{\rm cc} \simeq 1/2$ and $Q_{\rm cs} \simeq 0$. As for $q_{\rm cc}$s, for $\alpha < \beta$, $q_{\rm cc}^{\alpha\beta} \simeq q_{\rm ss}^{\alpha\beta}$, $q_{\rm cs}^{\alpha\beta} + q_{\rm sc}^{\alpha\beta} \simeq 0$, or $q_{\rm cc}^{\alpha\beta} + q_{\rm ss}^{\alpha\beta} \simeq 0$, $q_{\rm cs}^{\alpha\beta} \simeq q_{\rm sc}^{\alpha\beta}$. By $\phi_j^{\beta\prime} = \pi/2 - \phi_j^{\beta\prime}$, the latter becomes the former. Theoretically, both cases of $\alpha < \beta$ and $\beta < \alpha$ are taken into account for $q_{\rm cs}$. That is, for $\alpha \neq \beta$, $q_{\rm cs}^{\alpha,\beta}$ should be defined as $\frac{1}{N}\sum_j \cos\phi^\alpha \sin\phi^\beta$. Thus, numerical result $q_{\rm cs}^{\alpha\beta} + q_{\rm sc}^{\alpha\beta} \simeq 0$ confirms the theoretical result $q_{\rm cs} = 0$, and the assumption $q_{\rm cc}q_{\rm ss} > (\frac{q_{\rm cs}+q_{\rm sc}}{2})^2$ is satisfied. Also, if necessary, by transforming variables, the other assumptions $q_{\rm cc} > 0, q_{\rm ss} > 0$ are satisfied.

Also, numerically solving the SPEs for $q_{\rm cc}, q_{\rm ss}$, and $q_{\rm cs}$ with $Q_{\rm cc} = Q_{\rm ss} = \frac{1}{2}, Q_{\rm cs} = 0$, we obtain $q_{\rm cc} \simeq q_{\rm ss}$ and $q_{\rm cs} \simeq 0$. Taking these results into account, we set $q_{\rm cc} = q_{\rm ss}$ and $q_{\rm cs} = q_{\rm sc} = 0$ and obtain

$$
q = 2q_{\rm cc}. \qquad (14)
$$

In the Appendix, we prove that q obeys the same equation as that derived by Sherrington and Kirkpatrick [10]:

$$
q = 1 - \frac{k_{\rm B}T}{J}\sqrt{\frac{2}{q}}\int_0^\infty dr r^2 e^{-\frac{1}{2}r^2}\frac{I_1\left(\frac{J}{k_{\rm B}T}\sqrt{\frac{q}{2}}r\right)}{I_0\left(\frac{J}{k_{\rm B}T}\sqrt{\frac{q}{2}}r\right)}. \qquad (15)
$$

I_n is the nth order modified Bessel function of the first kind. The critical temperature is $T_c = J/2$ below which the spin glass phase appears.

III. NUMERICAL SIMULATION

Here, we show numerical results. In this paper, we set $J = 1$ and then $T_c = 0.5$.

A. Spin glass order parameter q

1. XY *model*

Now, let us explain our method of numerical calculations. We use the replica exchange Monte Carlo (REMC) method. We prepare 48 sets and 96 sets of temperature for $N = 100$ and 500, respectively, and a replica is assigned to each temperature. We call it a temperature replica. The temperature T ranges from 0.02 to 0.96 with the increment $\Delta T = 0.02$ for $N = 100$ and $\Delta T = 0.01$ for $N = 500$, respectively. In order to calculate q, we prepare another set of replicas. Two sets of replicas are denoted by α and β, respectively. The initial values of $\{\phi_j\}$ of all replicas are set to values in $[0, 2\pi)$ randomly. For $N = 100$ (500), we exchange temperature replicas every 5000 (1000) Monte Carlo (MC) sweeps. One MC sweep corresponds to N updates of spins. The number of exchanges is 10 000. After 500 exchanges, at each temperature, we calculate the time average of q using 100 sets of phases of XY spins for the last 100 MC sweeps during 5000 and 1000 MC sweeps for $N = 100$ and 500, respectively. We denote this average by $\bar{q}$. Then we take the average of $\bar{q}$ over 9500 exchanges, which we regard as the thermal average $\langle q\rangle$. At each temperature, the sample average of $\langle q\rangle$ and its standard deviation are calculated. The number of samples is 30 and 5

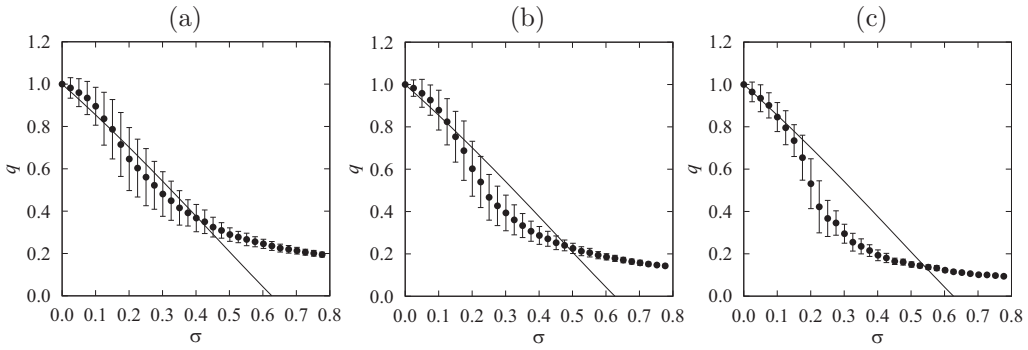

FIG. 2. σ dependence of the sample average of q in the phase oscillator network. (a) $N = 100$. (b) $N = 200$. (c) $N = 500$.

for $N = 100$ and for 500, respectively. We show the results of the temperature dependence of q in Fig. 1(a) for $N = 100$ and in Fig. 1(b) for $N = 500$. The solid curves are the theoretical results at the thermodynamic limit of $N = \infty$. The theoretical curves look straight, but they are slightly curved. The black circles are the sample average of q and the error bars are the standard deviation. The theoretical curves and the computer simulation results almost agree with each other at $T < 0.3$ for $N = 100$ and at $T < 0.4$ for $N = 500$, respectively. Therefore, it is expected that the agreement between the theoretical curves and the simulation results becomes better as N is increased, and the critical temperature will be $T_c = 0.5$, which is the theoretical result.

2. Phase oscillator network

We adopt the same definition of q by Eq. (4) as in the XY model. The computer simulation is carried out by the following method. In order to integrate Eq. (2) numerically, we adopt the Euler method with time increment $\Delta t = 0.02$. Since the Hamiltonian is not defined for the phase oscillator network, it is impossible to use the REMC method. Therefore, in analogy to the simulated annealing method, the relaxation calculation is carried out while gradually lowering σ from $1.5\sqrt{\pi/2}$ to zero with the increment $\Delta\sigma = 0.01\sqrt{\pi/2}$ for $N = 100$, $\Delta\sigma = 0.005\sqrt{\pi/2}$ for $N = 200$, and $\Delta\sigma = 0.000125\sqrt{\pi/2}$ for $N = 500$. In this paper, we also call this the simulated annealing method. At each σ, we evolve the system until $t = 800$ and calculate the time average of q using phases of oscillators from $t = 501$ to 800 with time interval 1. We denote this by $\bar{q}$. At each σ, the sample average of $\bar{q}$ and the standard deviation over samples are calculated. For this simulated annealing method, ω_j $(1 \leqslant j \leqslant N)$ is not generated for every σ. Instead, first, ω_j with $\sigma = 1$ is generated according to $\mathcal{N}(0, 1)$. We denote it $\omega_{j,0}$. Then, ω_j with $\sigma(\neq 1)$ is defined as $\sigma\omega_{j,0}$. The initial values of ϕ_j $(1 \leqslant j \leqslant N)$ at the beginning of the simulated annealing method are chosen randomly from $[0, 2\pi)$. In the simulated annealing method, there may be cases that the relaxed state is captured at a local minimum for $\sigma = 0$. In order to judge whether the relaxed state reaches the global minimum at $\sigma = 0$, we use the fact that the phase oscillator network with $\sigma = 0$ and the XY model with $T = 0$ are the same model. Concretely, we use the following method. We prepare the same interaction for both models. In the oscillator network, we choose two replicas with $q \simeq 1$ at $\sigma \sim 0$ obtained by the simulated annealing method. Then, we calculate q using ϕ_j $(1 \leqslant j \leqslant N)$ of one of two replicas of the phase oscillator network at $\sigma \sim 0$ and ϕ_j $(1 \leqslant j \leqslant N)$ of the XY model at the corresponding temperature $T = \sqrt{\frac{2}{\pi}}\sigma$ obtained by the REMC method. If $q > 0.99$, it is judged that the two replicas in the oscillator network reach the global minimum.

By this procedure, we obtain 100 ($N = 100$), 100 ($N = 200$), and 20 ($N = 500$) pairs of replicas which reach the global minimum at $\sigma \sim 0$.

Using these pairs, we calculate the sample average of $\bar{q}$ and the standard deviation. In Fig. 2, we display the σ dependence of the sample average of q with its standard deviation. The solid curve is obtained by the theoretical formula of q for the XY model by setting $\sigma = T\sqrt{\pi/2}$. For $\sigma < 0.4$ when $N = 100$, $\sigma < 0.2$ when $N = 200$, and $\sigma < 0.17$ when

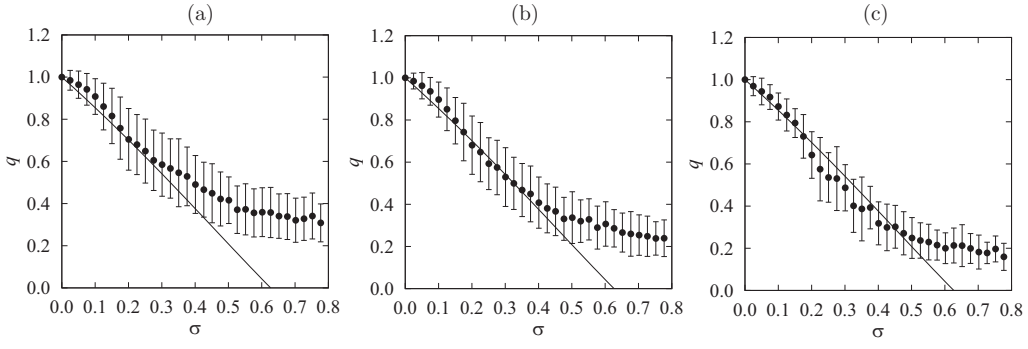

FIG. 3. σ dependence of the sample average of $q_{\rm av}$ in the phase oscillator network. (a) $N = 100$. (b) $N = 200$. (c) $N = 500$.

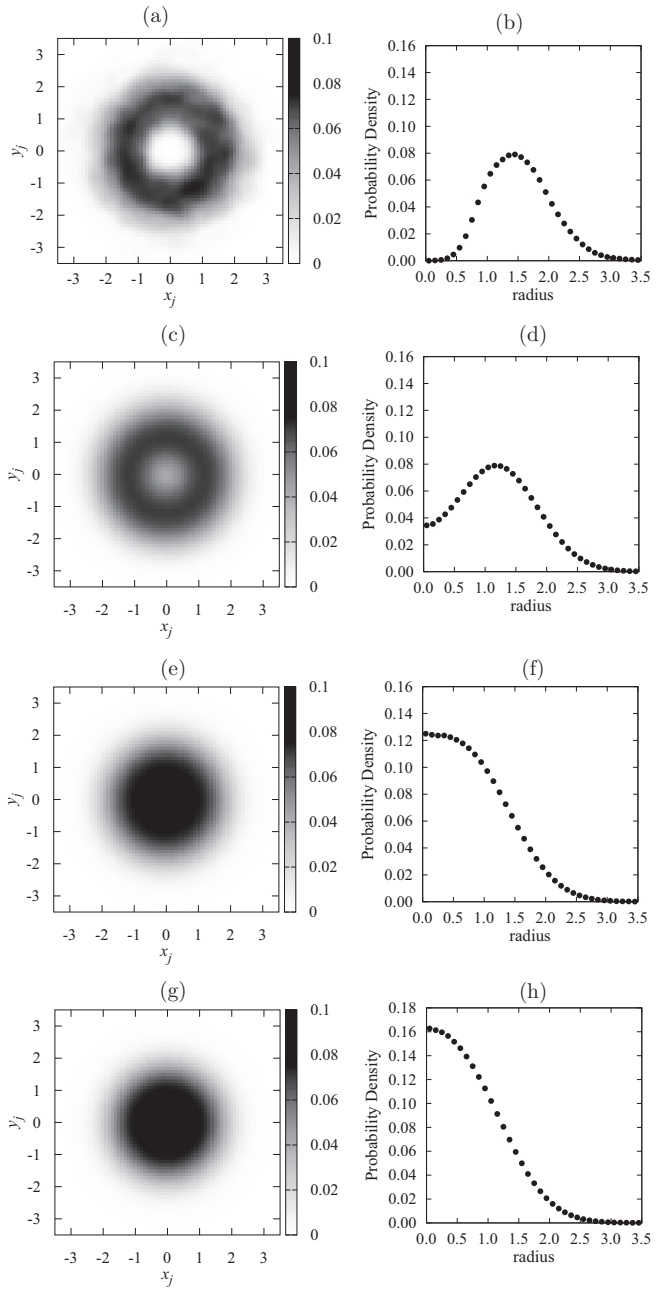

FIG. 4. Local field of the XY model ($N = 500$). Left panel: Spatial distribution of LFs on the complex plane. Right panel: Probability density of LFs, $P(r)$. (a, b) $T = 0.04$. (c, d) $T = 0.26$. (e, f) $T = 0.5$. (g, h) $T = 0.6$.

$N = 500$, the theoretical curve and the simulation results almost agree. However, contrary to our expectation, as the system size increases, the coinciding range of the theoretical curve and the simulation results decreases. The reason for this is considered to be that ϕ_j behaves intermittently in time as we show later in Fig. 7.

When we observe the time evolution of the LF, this is understood more explicitly. When σ is large, the amplitudes R_js and phases Θ_js of the LF fluctuate for some short time scale, and for a long time scale Θ_js evolve almost linearly. See Figs. 9 and 11.

Since we have interest in behavior for long periods, it is meaningful to observe time averaged quantities.

Therefore, we introduce the following quantity $q_{\rm av}$ for two replicas $\{\phi_j^\alpha\}$ and $\{\phi_j^\beta\}$:

$$q_{\rm av} = {\rm Max}\left(\frac{\left|\sum_{j=1}^N \bar{A}_j^\alpha \bar{A}_j^\beta e^{i(\bar{\phi}_j^\alpha - \bar{\phi}_j^\beta)}\right|}{\sum_{j=1}^N \bar{A}_j^\alpha \bar{A}_j^\beta}, \frac{\left|\sum_{j=1}^N \bar{A}_j^\alpha \bar{A}_j^\beta e^{i(\bar{\phi}_j^\alpha + \bar{\phi}_j^\beta)}\right|}{\sum_{j=1}^N \bar{A}_j^\alpha \bar{A}_j^\beta} \right), \tag{16}$$

$$\bar{A}_j^\alpha e^{i\bar{\phi}_j^\alpha} = \frac{1}{T_s}\sum_{k=1}^{T_s} e^{i\phi_j^\alpha(t_k)}, \quad \bar{A}_j^\beta e^{i\bar{\phi}_j^\beta} = \frac{1}{T_s}\sum_{k=1}^{T_s} e^{i\phi_j^\beta(t_k)}, \tag{17}$$

where $T_s = 300$ and $t_k = 500 + k$. The normalization factor $\sum_{j=1}^N \bar{A}_j^\alpha \bar{A}_j^\beta$ is determined so that $q_{\rm av}$ becomes 1 when ϕ_j^α and ϕ_j^β are equal or their difference is constant for all j. The numerical results are shown in Fig. 3 for $N = 100$, 200, and 500.

We note that the theoretical result of q for the XY model and numerical results of $q_{\rm av}$ in the phase oscillator network agree fairly well, and as N increases the coinciding range of the theoretical curve and the simulation results increases, and the critical parameter will be $\sigma_c = T_c\sqrt{\pi/2}$ when $N = \infty$. The results of T dependences of q in the XY model and σ dependences of q in the phase oscillator network imply that they differ by the factor $\sqrt{\pi/2}$ in the scale of abscissa axes as expected.

B. Local field

Now, let us study the local field $p_j = x_j + i\, y_j$ which is defined by

$$p_j = \sum_{k=1}^N J_{jk}\, e^{i\phi_k}. \tag{18}$$

LFs move on the complex plane with time due to the thermal fluctuation in the XY model, and in the phase oscillator network they move on the complex plane with time according to the evolution equation (2).

1. XY model

We numerically examine the spatial distribution of LFs on the complex plane for all spins. The initial values of ϕ_j ($1 \leqslant j \leqslant N$) are set as the final equilibrium state obtained when we calculate q. In Fig. 4, we display the distribution of LFs on the complex plane and the probability density $P(r)$ of LFs, where $r = \sqrt{x^2 + y^2}$. To draw Fig. 4, a Monte Carlo simulation is carried out for $N = 500$ and data are taken every one MC sweep during 10 000 MC sweeps. That is, $10\,000 \times N$ data are used to draw Fig. 4. When T is low, $P(r)$ is a volcanic shape with a hole in the center, i.e., $r = 0$, and the hole gradually closes with the increase of T, and then it disappears and the peak position becomes $r = 0$ for $T > 0.5 (= T_c)$.

2. Phase oscillator network

We calculate LFs as in the XY model. The initial values of ϕ_j ($1 \leqslant j \leqslant N$) are set as the final state obtained when we calculate q. In Fig. 5, we display the distribution of LFs

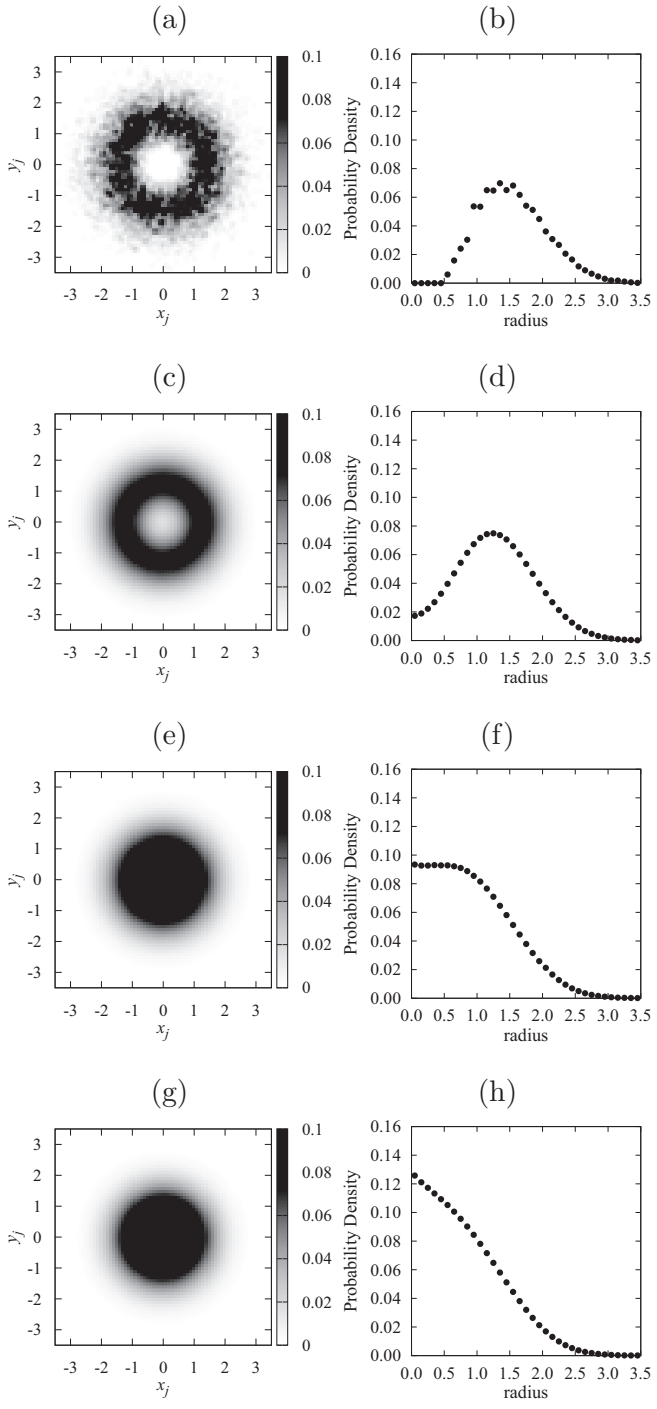

FIG. 5. The local field of the phase oscillator network ($N = 500$). Left panel: Spatial distribution on the complex plane. Right panel: Probability density $P(r)$. (a, b) $\sigma = 0.04\sqrt{\pi/2}$. (c, d) $\sigma = 0.26\sqrt{\pi/2}$. (e, f) $\sigma = 0.5\sqrt{\pi/2}$. (g, h) $\sigma = 0.6\sqrt{\pi/2}$.

and $P(r)$. A computer simulation is carried out for $N = 500$ until $t = 10\,000$, and data are taken every time interval 1 to draw Fig. 5. That is, the number of data to draw Fig. 5 is the same as in the XY model. As is seen from Fig. 5, with the increase of σ from zero, behavior of $P(r)$ is the same as in the XY model and the peak position becomes $r = 0$ for $\sigma > 0.5\sqrt{\pi/2}(= T_c\sqrt{\pi/2})$.

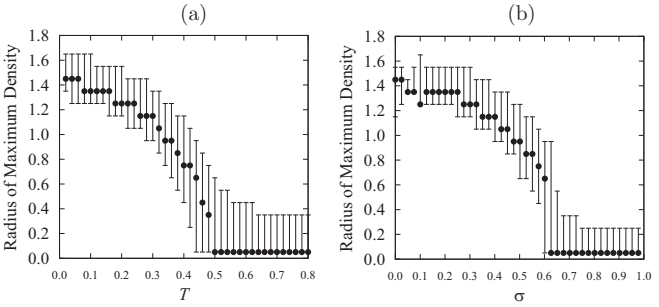

FIG. 6. Temperature dependence of the peak radius r_p in the XY model ($N = 500$) and σ dependence of r_p in the phase oscillator network ($N = 500$). (a) XY model. (b) Phase oscillator.

3. Comparison of results for both models

In the LFs of the XY model, for $N = 500$, the T dependence of the radius at which the probability density has a peak is shown in Fig. 6(a). We call the radius the peak radius, and denote it by r_p. The black circles show the peak radius, and the error bars show the radius at which the probability density decreases by 5% from the peak. The peak radius at $T > 0.5(= T_c)$ becomes nearly zero. In the LFs of the phase oscillator network, for $N = 500$, the σ dependence of the peak radius is shown in Fig. 6(b). The circles and error bars have

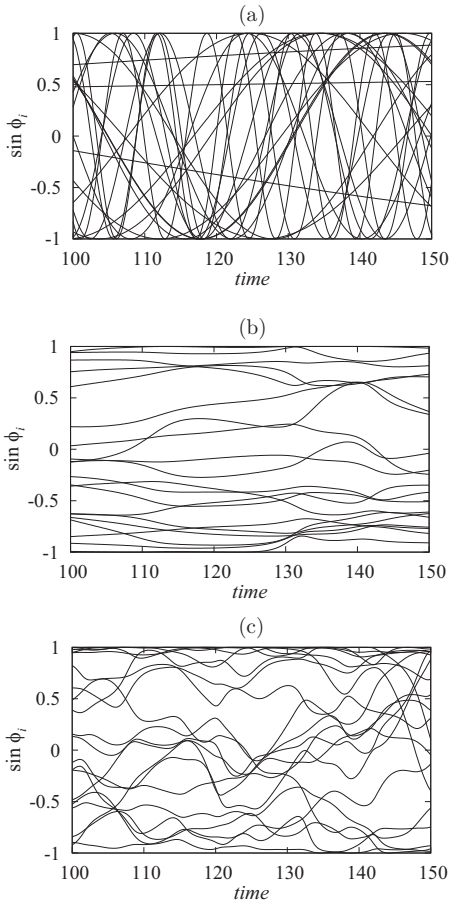

FIG. 7. Time series of $\sin\phi(t)$. $N = 100$. (a) $J_{jk} = 0$. (b) $J_{jk} \neq 0$, $\sigma = 0.2$. (c) $J_{jk} \neq 0$, $\sigma = 0.3$.

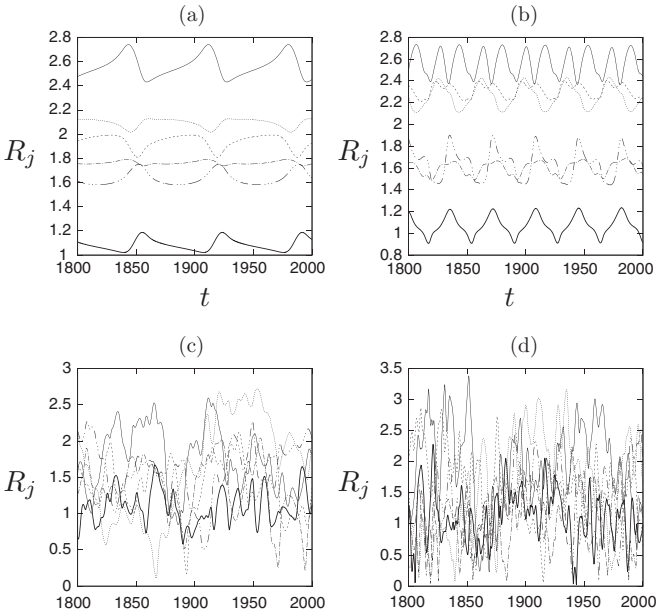

FIG. 8. Time series of R_js for several oscillators. $N = 200$. (a) $\sigma = 0.1\sqrt{0.5\pi}$. (b) $\sigma = 0.2\sqrt{0.5\pi}$. (c) $\sigma = 0.3\sqrt{0.5\pi}$. (d) $\sigma = 0.5\sqrt{0.5\pi}$.

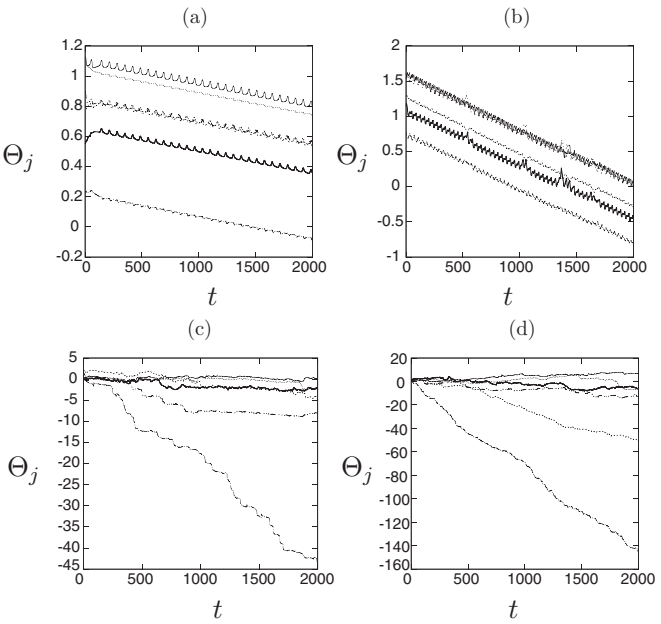

FIG. 9. Time series of Θ_js for several oscillators. $N = 200$. (a) $\sigma = 0.1\sqrt{0.5\pi}$. (b) $\sigma = 0.2\sqrt{0.5\pi}$. (c) $\sigma = 0.3\sqrt{0.5\pi}$. (d) $\sigma = 0.5\sqrt{0.5\pi}$.

the same meanings as in the XY model. The peak radius at $\sigma > 0.5\sqrt{\pi/2}(= T_c\sqrt{\pi/2})$ becomes nearly zero. T and σ in which the peak radius becomes zero seem to differ by the factor $\sqrt{\pi/2}$ in the scale of abscissa axes as expected.

C. Numerical results for several quantities in the phase oscillator network

In the phase oscillator network, in order to study the roles of synchronous and asynchronous oscillators for the correspondence, we numerically calculate several quantities. First, we study the time evolution of $\sin\phi$ where ϕ is the phase of each oscillator. In Fig. 7, we show $\sin\phi(t)$ of 20 oscillators for $N = 100$ during $t = 0$–150. In Fig. 7(a), we set $J_{jk} = 0$, that is, $\phi_j = \omega_j t + \phi_j(0)$. In Figs. 7(b) and 7(c), we set $J_{jk} \neq 0$, and $\sigma = 0.2\sqrt{\frac{\pi}{2}}$ and $0.3\sqrt{\frac{\pi}{2}}$, respectively. We note that oscillators are locked for a while and then are unlocked, and repeat this behavior. We find that, the larger σ is, the more fluctuations of phases there are, and trajectories behave chaotically. Next, we study trajectories of LFs for a long time for $N = 200$ and 500. See Figs. 8–11. We define the amplitude R_j and phase Θ_j of the LFs by

$$R_j e^{i\Theta_j} = p_j = \sum_k J_{jk} e^{i\phi_k}. \tag{19}$$

In this simulation, we adopt the simulated annealing and the schedule is $T_l = 0.7 - (l-1) \times 0.02$, $l = 1$–35. We obtain the following results. When σ is small, $\sigma < \sigma_{c1}$, R_j and Θ_j are constant or periodic depending on N. The distribution of substantial frequencies is $G(\tilde{\omega}) = \delta(\tilde{\omega})$. When σ becomes large, $\sigma_{c1} < \sigma < \sigma_{c2}$, R_j behaves chaotically, and Θ_j has two phases. Θ_j is almost constant in one phase, and it increases or decreases rapidly in the other phase. On average, Θ_j evolves almost linearly. When σ is large enough, $\sigma_{c2} < \sigma$, Θ_j evolves almost linearly. It seems that σ_{c1} and σ_{c2} depend on N. For N that we investigated, $\sigma_{c1} \sim 0.1\sqrt{\frac{\pi}{2}}$.

$G(\tilde{\omega})$ is one-humped and continuous, and it is impossible to separate synchronized oscillators from desynchronized ones. See Fig. 12.

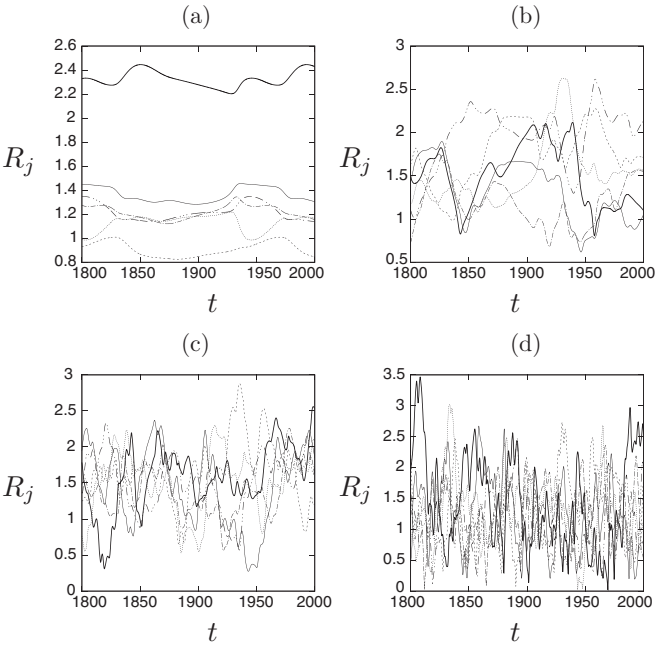

FIG. 10. Time series of R_js for several oscillators. $N = 500$. (a) $\sigma = 0.1\sqrt{0.5\pi}$. (b) $\sigma = 0.2\sqrt{0.5\pi}$. (c) $\sigma = 0.3\sqrt{0.5\pi}$. (d) $\sigma = 0.5\sqrt{0.5\pi}$.

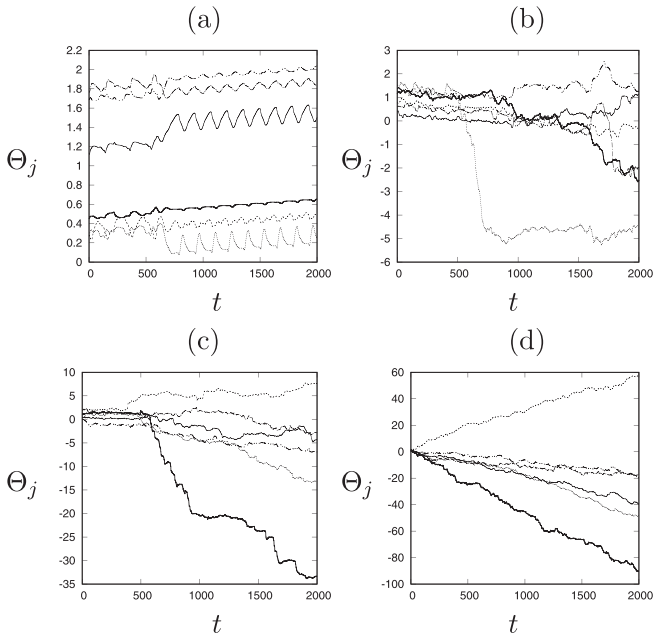

FIG. 11. Time series of Θ_js for several oscillators. $N = 500$. (a) $\sigma = 0.1\sqrt{0.5\pi}$. (b) $\sigma = 0.2\sqrt{0.5\pi}$. (c) $\sigma = 0.3\sqrt{0.5\pi}$. (d) $\sigma = 0.5\sqrt{0.5\pi}$.

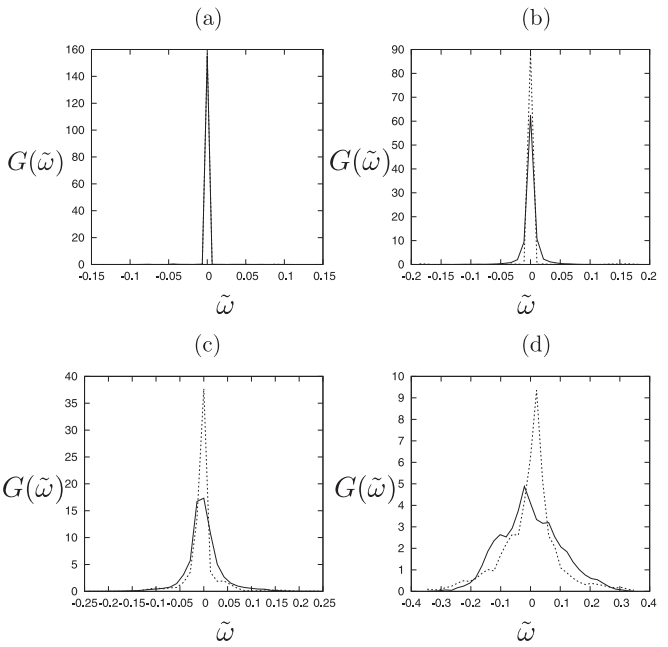

FIG. 12. Probability density of substantial frequency $\tilde{\omega}_j$ of Θ_j, $G(\tilde{\omega})$. Solid curve, $N = 500$; dashed curve, $N = 200$. (a) $\sigma = 0.1\sqrt{0.5\pi}$. (b) $\sigma = 0.2\sqrt{0.5\pi}$. (c) $\sigma = 0.3\sqrt{0.5\pi}$. (d) $\sigma = 0.5\sqrt{0.5\pi}$.

In the next subsection, we derive the self-consistent equations for LFs in the *XY* model and oscillator network by using approximations.

D. SCE for LFs

In the oscillator network, we derive the SCE for the case that all oscillators are synchronized. In the *XY* model, we derive the SCE by using the naive mean-field approximation.

1. Oscillator network

Using R_j and Θ_j, the evolution equation is rewritten as

$$\frac{d}{dt}\phi_j = \omega_j - R_j \sin(\phi_j - \Theta_j). \tag{20}$$

R_j and Θ_j are constant because all oscillators are assumed to be synchronized. Thus, by defining $\psi_j = \phi_j - \Theta_j$, we obtain

$$\frac{d}{dt}\psi_j = \omega_j - R_j \sin\psi_j. \tag{21}$$

The stable solution is $\psi_j^* = \sin^{-1}\frac{\omega_j}{R_j}$ where $|\psi_j^*| < \frac{\pi}{2}$. The probability density function of phases $f(\psi;\omega_j)$ is $\delta(\psi - \psi_j^*)$. Thus, the average of $e^{i\phi_j}$ is

$$\langle e^{i\phi_j}\rangle = e^{i(\psi_j^* + \Theta_j)} = \left[\sqrt{1 - \left(\frac{\omega_j}{R_j}\right)^2} + i\frac{\omega_j}{R_j}\right]e^{i\Theta_j}. \tag{22}$$

Therefore, the SCE for LFs is

$$R_j e^{i\Theta_j} = \sum_{j'=1}^{N} J_{jj'}\left[\sqrt{1 - \left(\frac{\omega_{j'}}{R_{j'}}\right)^2} + i\frac{\omega_{j'}}{R_{j'}}\right]e^{i\Theta_{j'}}. \tag{23}$$

We numerically solve the SCE (23) by iteration method. That is, from $\{R_j\}$ and $\{\Theta_j\}$ at iteration step n, we evaluate the right-hand side of Eq. (23) to obtain $\{R_j\}$ and $\{\Theta_j\}$ at iteration step $n+1$. We define the distance between two configurations $\{\phi_j\}$ and $\{\phi'_j\}$ as

$$d(\{\phi_j\},\{\phi'_j\}) \equiv \sum_{j=1}^{N} |\phi_j - \phi'_j|.$$

The convergence condition is $d(\{\phi_j(n)\},\{\phi_j(n+1)\}) < \epsilon$ for two successive configurations $\{\phi_j(n)\}$ and $\{\phi_j(n+1)\}$ with $\epsilon = 0.01$. It turns out that it is very difficult to obtain solutions for Eq. (23) if initial conditions are taken randomly. Then, as an initial condition, we use the numerical results obtained by the simulated annealing method, and find that almost all numerical results are solutions of the SCE when σ is small. For example, we find that when $N = 100$ and $\sigma = 0.02\sqrt{\frac{\pi}{2}}$ all 19 configurations obtained by the simulated annealing converge by only one iteration and $d(\{\phi_j(0)\},\{\phi_j(1)\}) \sim 3\times10^{-5}$, that is, these configurations satisfy Eq. (23). We regard two configurations $\{\phi_j\}$ and $\{\phi'_j\}$ to be different when $d(\{\phi_j\},\{\phi'_j\}) > \epsilon$. We find only two different configurations among 19 configurations. When $N = 100$ and $\sigma = 0.1\sqrt{\frac{\pi}{2}}$, we find that 16 configurations converge by only one iteration among 19 configurations, and all of them are regarded as the same. However, for larger values of σ, we cannot find any solution. This is because R_j and Θ_j are not constant and it seems that asynchronous solutions contribute to the LFs.

2. XY model

The Hamiltonian is

$$H = -\sum_{j<k} J_{jk}\cos(\phi_k - \phi_j) = -\frac{1}{2}\sum_j R_j \cos(\phi_j - \Theta_j). \tag{24}$$

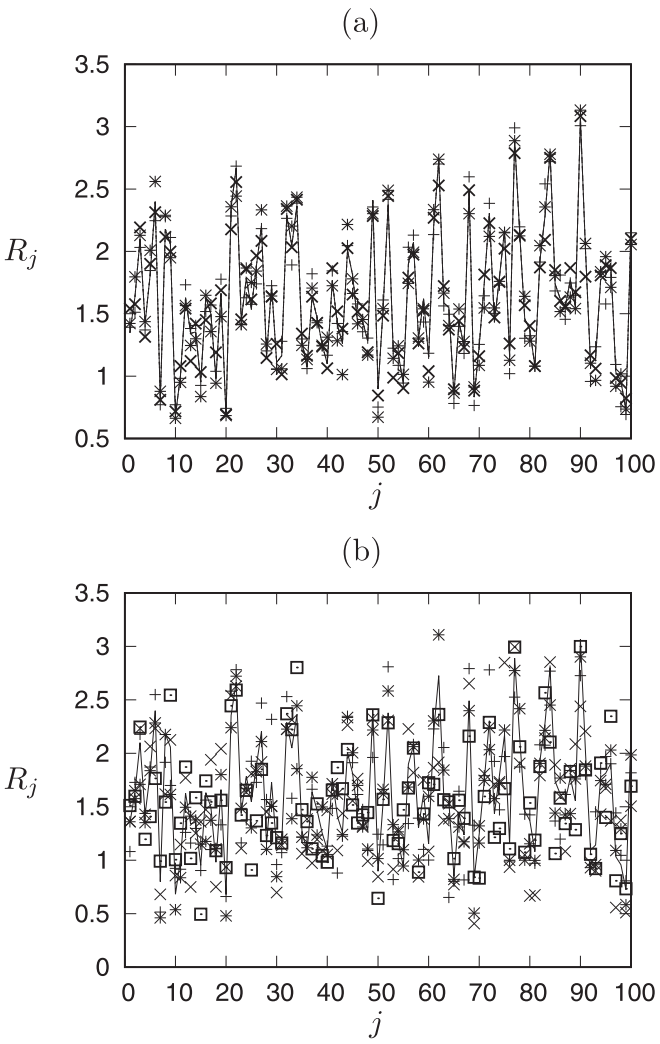

FIG. 13. j dependences of R_j. XY model. $N = 100$. Symbols, different solutions among convergent solutions obtained by the iteration of Eq. (26); broken line, initial condition which is the final value of the annealing. (a) $T = 0.02$, three different solutions. (b) $T = 0.1$, four different solutions.

Since the probability density function of phases is $P(\phi_j) = \frac{e^{\beta R_j \cos(\phi_j - \Theta_j)}}{2\pi I_0(\beta R_j)}$, defining $\psi_j = \phi_j - \Theta_j$ we obtain

$$\langle e^{i\phi_j} \rangle = \frac{1}{2\pi I_0(\beta R_j)} \int_0^{2\pi} e^{\beta R_j \cos\psi} e^{i(\psi + \Theta_j)} d\phi = \frac{I_1(\beta R_j)}{I_0(\beta R_j)} e^{i\Theta_j} = \beta R_j e^{i\Theta_j} u(\beta R_j). \quad (25)$$

Here, $u(x) = \frac{I_1(x)}{xI_0(x)}$. Thus, we obtain

$$R_j e^{i\Theta_j} = \sum_k J_{jk} \langle e^{i\phi_k} \rangle = \beta \sum_k J_{jk} R_k e^{i\Theta_k} u(\beta R_k). \quad (26)$$

As an initial condition, we use the configuration obtained by the simulated annealing as in the oscillator network. The method to solve Eq. (26), the convergence condition, and the criterion of different solutions are the same as in the phase oscillator network. When $N = 100$ and $T = 0.02$, among 30 configurations, three configurations converge with $\epsilon = 0.01$. The numbers of iterations are rather large compared to the oscillator network and are 29, 51, and 62 for these three configurations, respectively. All of them are different, but it is difficult to distinguish these three from the figure of j vs R_j. When $N = 100$ and $T = 0.1$, among 30 configurations, five configurations converge, and the number of iterations ranges from 50 to 70. Four configurations among five are different. We find that convergent values and initial conditions are rather different and this is consistent with the fact that the numbers of iterations are large. See Fig. 13. Therefore, in this case, final configurations by the simulated annealing for $T = 0.1$ are not considered as the solutions of the SCEs. The reason for this is considered to be that the naive mean-field approximation is not valid for high temperatures.

IV. SUMMARY AND DISCUSSION

We summarize the results of this paper. We studied the random and frustrated interaction, the SK interaction, which is generated by the Gaussian distribution with mean zero and standard deviation $J/\sqrt{N}$. As for the distribution of natural frequencies $g(\omega)$, we adopted the Gaussian distribution with mean zero and standard deviation σ. In order to study whether correspondence between the two models exists or not, we performed numerical calculations of the spin glass order parameter q and the distributions of the LFs in the XY model and phase oscillator network. In the XY model, we used the Markov chain Monte Carlo simulation, in particular, the REMC method and the simulated annealing method. In the oscillator network, we used the Euler method with time increment $\Delta t = 0.02$, and also used the simulated annealing method, that is, we integrated the evolution equation by decreasing σ slowly. First, we summarize the results of q. In the XY model, we confirmed that theoretical and numerical results agree fairly well and found that the coinciding region between the theoretical curve and the simulation results of q increases as N increases. For the phase oscillator network, we found that in the σ dependence of the spin glass order parameter the numerical results agree with the theoretical curve $q[T(\sigma)]$ of the XY model at least for lower values of σ in the spin glass phase. Here, $T(\sigma) = \sqrt{\frac{2}{\pi}}\sigma$ is the relation obtained in the previous paper [8]. However, the coinciding region between the simulation results and the theoretical curve decreases as N increases, contrary to our expectation. Since ϕ_j behaves intermittently in time, we introduced the order parameter $q_{\rm av}$ for the time averaged phases, and found that the coinciding region between the theoretical curve of the XY model and the simulation results of $q_{\rm av}$ increases as N increases.

Next, we summarize the results of LFs.

We studied the probability density $P(r)$ of LFs, where r is the radius of the local field in the complex plane. As T or σ increases, the peak radius r_p of $P(r)$ changes from a nonzero value to zero. This is the so called volcano transition, and the transition points of the two models seem to correspond according to the relation $T = \sqrt{\frac{2}{\pi}}\sigma$. For the oscillator network, we numerically studied time evolution of $\sin\phi_i$ of each oscillator and found that oscillators are locked for a while and then are unlocked, and repeat this behavior. We also numerically studied time evolution of amplitudes Rs and

phases Θs of LFs. We found that when σ is small they are constant or periodic depending on N, and the distribution of the substantial frequencies $G(\tilde{\omega})$ is the delta function $\delta(\tilde{\omega})$, but, when σ is large, R_j behaves chaotically, and Θ_j has two phases: in one phase Θ_j is almost constant, and in the other phase it increases or decreases rapidly. On average, Θ_j evolves almost linearly. $G(\tilde{\omega})$ is one-humped and continuous.

Finally, we derived the SCE of LFs for the oscillator network in the case that all oscillators synchronize and for the XY model by using the naive mean-field approximation. We found that for the oscillator network and XY model, when σ and T are small, configurations obtained by simulated annealing satisfy the SCE, but when σ and T are large they do not. The reasons for the discrepancy between theoretical and numerical results for the LFs at large T and σ are considered to be as follows. In the oscillator network, the asynchronous oscillators do not contribute to the LFs for the solvable models when the $g(\omega)$ is one-humped and symmetric with respect to its center. However, the present results imply that asynchronous oscillators contribute to the LFs. Since $G(\omega)$ is continuous, it is difficult to separate synchronized oscillators from desynchronized ones. In the XY model, the present results imply that the naive mean-field approximation is not valid except for very low temperatures. This is the same as in the case of Ising spins. The so called Onsager reaction field should be taken into account for the XY model as in the Ising model. Therefore, in order to improve the present approximations for the two models, further elaborate studies are necessary, and these studies are beyond the scope of the present paper and are left as a future problem.

Here, we discuss the reason why $q_{\rm av}$ agrees better with the theoretical result of the XY model than the simple time average of q in the phase oscillator network. $\{\phi_j\}$, local fields, and $\{e^{\phi_j^\alpha(t)}\}$ behave intermittently in time. For larger σ and larger N in the spin glass phase, the intermittent behavior becomes stronger. As is seen from Fig. 2, the agreement between the simulation results and the theoretical curve becomes worse for larger values of σ as N is increased. Since the number of desynchronized oscillators increases as σ increases as evidenced by Fig. 12, one of the causes of the disagreement might be that the contribution of the desynchronized oscillators to the overlap is not evaluated appropriately due to their intermittent behavior, and, as a result, the time average of the overlap between $\{e^{\phi_j^\alpha(t)}\}$ and $\{e^{\phi_j^\beta(t)}\}$ is reduced. On the other hand, as noted from Fig. 3, by using the time averaged quantities $\{\bar{A}_j^\alpha e^{i\bar{\phi}_j^\alpha}\}$ and $\{\bar{A}_j^\beta e^{i\bar{\phi}_j^\alpha}\}$, the reduction of the overlap due to such intermittent behavior seems to weaken. However, in order to obtain a definite conclusion, more investigations on this subject are necessary. This is left as another future problem.

ACKNOWLEDGMENTS

The present paper is supported by Japan Society for the Promotion of Science KAKENHI Grants No. 16K05474, No. 25330298, and No. 17K00357.

APPENDIX

In this Appendix, we derive the disorder averaged free energy per spin and the SPEs under the ansatz of replica symmetry. The derivation is based on Ref. [12]:

$$\bar{f} = -\lim_{N\to\infty}\lim_{n\to 0}(\beta N n)^{-1}\log\int d\boldsymbol{\phi}^1\cdots\boldsymbol{\phi}^n\overline{e^{-\beta\sum_\alpha H(\boldsymbol{\phi}^\alpha)}}, \tag{A1}$$

$$\overline{e^{-\beta\sum_\alpha H(\boldsymbol{\phi}^\alpha)}} = \exp\left[\frac{\beta^2J^2}{4N}\sum_{\alpha\beta}\left\{\left(\sum_i\cos\phi_i^\alpha\cos\phi_i^\beta\right)^2+\left(\sum_i\sin\phi_i^\alpha\sin\phi_i^\beta\right)^2+\left(\sum_i\cos\phi_i^\alpha\sin\phi_i^\beta\right)^2 + \left(\sum_i\sin\phi_i^\alpha\cos\phi_i^\beta\right)^2 - N\right\}\right], \tag{A2}$$

where $\boldsymbol{\phi}^\alpha = (\phi_1^\alpha,\cdots,\phi_N^\alpha)$. We define the following order parameters. For $\alpha<\beta$,

$$q_{\rm cc}^{\alpha\beta} = \frac{1}{N}\sum_i\cos\phi_i^\alpha\cos\phi_i^\beta,\ q_{\rm ss}^{\alpha\beta} = \frac{1}{N}\sum_i\sin\phi_i^\alpha\sin\phi_i^\beta,$$

$$q_{\rm cs}^{\alpha\beta} = \frac{1}{N}\sum_i\cos\phi_i^\alpha\sin\phi_i^\beta,\ q_{\rm sc}^{\alpha\beta} = \frac{1}{N}\sum_i\sin\phi_i^\alpha\cos\phi_i^\beta,$$

and for $\alpha = 1,\cdots,n$

$$Q_{\rm cc}^{\alpha} = \frac{1}{N}\sum_i\cos^2\phi_i^\alpha,\ Q_{\rm ss}^{\alpha} = \frac{1}{N}\sum_i\sin^2\phi_i^\alpha,\ Q_{\rm cs}^{\alpha} = \frac{1}{N}\sum_i\cos\phi_i^\alpha\sin\phi_i^\alpha.$$

Then, we obtain

$$\overline{e^{-\beta\sum_\alpha H(\boldsymbol{\phi}^\alpha)}} = e^{-\frac{\beta^2J^2n^2}{4}}\exp\left[\frac{\beta^2J^2N}{4}\sum_\alpha\left\{\left(Q_{\rm cc}^\alpha\right)^2+\left(Q_{\rm ss}^\alpha\right)^2+2\left(Q_{\rm cs}^\alpha\right)^2\right\}+2\sum_{\alpha<\beta}\left\{\left(q_{\rm cc}^{\alpha\beta}\right)^2+\left(q_{\rm ss}^{\alpha\beta}\right)^2+\left(q_{\rm cs}^{\alpha\beta}\right)^2+\left(q_{\rm sc}^{\alpha\beta}\right)^2\right\}\right]. \tag{A3}$$

Using the integral representation of δ functions such as

$$\int \frac{1}{2\pi} dq_{\rm cc}^{\alpha\beta} d\hat{q}_{\rm cc}^{\alpha\beta} e^{i\hat{q}_{\rm cc}^{\alpha\beta}(q_{\rm cc}^{\alpha\beta} - \frac{1}{N}\sum_i \cos\phi_i^\alpha \cos\phi_i^\beta)} = 1,$$

and rescaling variables as $\hat{q}_{\rm cc}^{\alpha\beta} \to N\hat{q}_{\rm cc}^{\alpha\beta}$, $\hat{Q}_{\rm cc}^{\alpha} \to N\hat{Q}_{\rm cc}^{\alpha}$, etc., we obtain

$$\bar{f} = -\lim_{N\to\infty}\lim_{n\to 0}(\beta N n)^{-1}\log\left\{\int d\boldsymbol{q} e^{N(\Phi+\Psi)}\right\}, \tag{A4}$$

$$\begin{aligned}\Phi = {} & i\sum_\alpha \left\{\hat{Q}_{\rm cc}^\alpha Q_{\rm cc}^\alpha + \hat{Q}_{\rm ss}^\alpha Q_{\rm ss}^\alpha + \hat{Q}_{\rm cs}^\alpha Q_{\rm cs}^\alpha\right\} + i\sum_{\alpha<\beta}\left\{\hat{q}_{\rm cc}^{\alpha\beta} q_{\rm cc}^{\alpha\beta} + \hat{q}_{\rm ss}^{\alpha\beta} q_{\rm ss}^{\alpha\beta} + \hat{q}_{\rm cs}^{\alpha\beta} q_{\rm cs}^{\alpha\beta} + \hat{q}_{\rm sc}^{\alpha\beta} q_{\rm sc}^{\alpha\beta}\right\} \\ & + \frac{\beta^2 J^2}{4}\left\{\sum_\alpha\left[\left(Q_{\rm cc}^\alpha\right)^2 + \left(Q_{\rm ss}^\alpha\right)^2 + 2\left(Q_{\rm cs}^\alpha\right)^2\right] + 2\sum_{\alpha<\beta}\left[\left(q_{\rm cc}^{\alpha\beta}\right)^2 + \left(q_{\rm ss}^{\alpha\beta}\right)^2 + \left(q_{\rm cs}^{\alpha\beta}\right)^2 + \left(q_{\rm sc}^{\alpha\beta}\right)^2\right]\right\},\end{aligned}$$

$$\begin{aligned}\Psi = {} & \frac{1}{N}\log\left\{\left[\int\prod_\alpha d\boldsymbol{\phi}^\alpha\right]\exp\left[-i\sum_\alpha\sum_i\left(\hat{Q}_{\rm cc}^{\alpha\beta}\cos^2\phi_i^\alpha + \hat{Q}_{\rm ss}^{\alpha\beta}\sin^2\phi_i^\alpha + \hat{Q}_{\rm cs}^{\alpha\beta}\cos\phi_i^\alpha\sin\phi_i^\alpha\right)\right. \right. \\ & \left.\left. - i\sum_{\alpha<\beta}\sum_i\left(\hat{q}_{\rm cc}^{\alpha\beta}\cos\phi_i^\alpha\cos\phi_i^\beta + \hat{q}_{\rm ss}^{\alpha\beta}\sin\phi_i^\alpha\sin\phi_i^\beta + \hat{q}_{\rm cs}^{\alpha\beta}\cos\phi_i^\alpha\sin\phi_i^\beta + \hat{q}_{\rm sc}^{\alpha\beta}\sin\phi_i^\alpha\cos\phi_i^\beta\right)\right]\right\},\end{aligned} \tag{A5}$$

where $d\boldsymbol{q} = \prod_\alpha(\frac{N d\hat{Q}_{\rm cc}^\alpha dQ_{\rm cc}^\alpha}{2\pi}\frac{N d\hat{Q}_{\rm ss}^\alpha dQ_{\rm ss}^\alpha}{2\pi}\frac{N d\hat{Q}_{\rm cs}^\alpha dQ_{\rm cs}^\alpha}{2\pi})\prod_{\alpha<\beta}(\frac{N d\hat{q}_{\rm cc}^{\alpha\beta} dq_{\rm cc}^{\alpha\beta}}{2\pi}\frac{N d\hat{q}_{\rm ss}^{\alpha\beta} dq_{\rm ss}^{\alpha\beta}}{2\pi}\frac{N d\hat{q}_{\rm cs}^{\alpha\beta} dq_{\rm cs}^{\alpha\beta}}{2\pi}\frac{N d\hat{q}_{\rm sc}^{\alpha\beta} dq_{\rm cs}^{\alpha\beta}}{2\pi})$. Since we consider $N\to\infty$, the integration is estimated by the saddle point of $\Phi+\Psi$:

$$\bar{f} = -\lim_{N\to\infty}\lim_{n\to 0}(\beta N n)^{-1}\log\left\{\int d\boldsymbol{q} e^{N(\Phi+\Psi)}\right\} \sim -\lim_{n\to 0}(\beta n)^{-1}\,\mathrm{extr}\,(\Phi+\Psi). \tag{A6}$$

Now, let us consider the replica symmetric solution:

$$Q_{\rm cc}^\alpha = Q_{\rm cc},\ Q_{\rm ss}^\alpha = Q_{\rm ss},\ Q_{\rm cs}^\alpha = Q_{\rm cs},\ \hat{Q}_{\rm cc}^\alpha = \hat{Q}_{\rm cc},\ \hat{Q}_{\rm ss}^\alpha = \hat{Q}_{\rm ss},\ \hat{Q}_{\rm cs}^\alpha = \hat{Q}_{\rm cs}, \tag{A7}$$

$$q_{\rm cc}^{\alpha\beta} = q_{\rm cc},\ q_{\rm ss}^{\alpha\beta} = q_{\rm ss},\ q_{\rm cs}^{\alpha\beta} = q_{\rm cs},\ \hat{q}_{\rm cc}^{\alpha\beta} = \hat{q}_{\rm cc},\ \hat{q}_{\rm ss}^{\alpha\beta} = \hat{q}_{\rm ss},\ \hat{q}_{\rm cs}^{\alpha\beta} = \hat{q}_{\rm cs}, \hat{q}_{\rm sc}^{\alpha\beta} = \hat{q}_{\rm sc}. \tag{A8}$$

Then, by changing conjugate variables from $\hat{q}_{\rm cc} \to i\hat{q}_{\rm cc}$, $\hat{Q}_{\rm cc} \to i\hat{Q}_{\rm cc}$, etc., we obtain

$$\begin{aligned}\lim_{n\to 0}\frac{1}{n}\Phi_{\rm RS} = {} & -(\hat{Q}_{\rm cc}Q_{\rm cc} + \hat{Q}_{\rm ss}Q_{\rm ss} + \hat{Q}_{\rm cs}Q_{\rm cs}) + \frac{1}{2}(\hat{q}_{\rm cc}q_{\rm cc} + \hat{q}_{\rm ss}q_{\rm ss} + \hat{q}_{\rm cs}q_{\rm cs} + \hat{q}_{\rm sc}q_{\rm sc}) \\ & + \frac{\beta^2 J^2}{4}\left(Q_{\rm cc}^2 + Q_{\rm ss}^2 + 2Q_{\rm cs}^2 - q_{\rm cc}^2 - q_{\rm ss}^2 - q_{\rm cs}^2 - q_{\rm sc}^2\right),\end{aligned} \tag{A9}$$

$$\lim_{n\to 0}\frac{1}{n}\Psi_{\rm RS} = \lim_{n\to 0}\frac{1}{n}\log\left(\int\left[\prod_\alpha d\phi^\alpha\right]e^L\right), \tag{A10}$$

$$\begin{aligned}L = {} & \sum_\alpha(\hat{Q}_{\rm cc}\cos^2\phi^\alpha + \hat{Q}_{\rm ss}\sin^2\phi^\alpha + \hat{Q}_{\rm cs}\cos\phi^\alpha\sin\phi^\alpha) \\ & + \sum_{\alpha<\beta}(\hat{q}_{\rm cc}\cos\phi^\alpha\cos\phi^\beta + \hat{q}_{\rm ss}\sin\phi^\alpha\sin\phi^\beta + \hat{q}_{\rm cs}\cos\phi^\alpha\sin\phi^\beta + \hat{q}_{\rm sc}\sin\phi^\alpha\cos\phi^\beta).\end{aligned} \tag{A11}$$

By using the Hubbard-Stratonovich transformation, e^L is rewritten as

$$\begin{aligned}e^L = {} & \exp\left[\left(\hat{Q}_{\rm cc} - \frac{1}{2}\hat{q}_{\rm cc}\right)\sum_\alpha\cos^2\phi^\alpha + \left(\hat{Q}_{\rm ss} - \frac{1}{2}\hat{q}_{\rm ss}\right)\sum_\alpha\sin^2\phi^\alpha + \left(\hat{Q}_{\rm cs} - \frac{\hat{q}_{\rm cs}+\hat{q}_{\rm sc}}{2}\right)\sum_\alpha\sin\phi^\alpha\cos\phi^\alpha\right] \\ & \times\int Dx\int Dy\exp\left[\sqrt{\frac{\hat{q}_{\rm cc}\hat{q}_{\rm ss} - \left(\frac{\hat{q}_{\rm cs}+\hat{q}_{\rm cs}}{2}\right)^2}{\hat{q}_{\rm ss}}}\sum_\alpha\cos\phi^\alpha\,x + \left(\frac{(\hat{q}_{\rm cs}+\hat{q}_{\rm sc})}{2\sqrt{\hat{q}_{\rm ss}}}\sum_\alpha\cos\phi^\alpha + \sqrt{\hat{q}_{\rm ss}}\sum_\alpha\sin\phi^\alpha\right)y\right],\end{aligned} \tag{A12}$$

where $Dx = (2\pi)^{-1/2}e^{-x^2/2}dx$. Then, we obtain

$$\begin{aligned}\lim_{n\to 0}\frac{1}{n}\Psi_{\rm RS} = {} & \int Dx\int Dy\log\int d\phi\exp\left[\left(\hat{Q}_{\rm cc} - \frac{1}{2}\hat{q}_{\rm cc}\right)\cos^2\phi + \left(\hat{Q}_{\rm ss} - \frac{1}{2}\hat{q}_{\rm ss}\right)\sin^2\phi + \left(\hat{Q}_{\rm cs} - \frac{\hat{q}_{\rm cs}+\hat{q}_{\rm sc}}{2}\right)\sin\phi\cos\phi\right. \\ & \left. + \sqrt{\frac{\hat{q}_{\rm cc}\hat{q}_{\rm ss} - \left(\frac{\hat{q}_{\rm cs}+\hat{q}_{\rm cs}}{2}\right)^2}{\hat{q}_{\rm ss}}}\cos\phi\,x + \left(\frac{\hat{q}_{\rm cs}+\hat{q}_{\rm sc}}{2\sqrt{\hat{q}_{\rm ss}}}\cos\phi + \sqrt{\hat{q}_{\rm ss}}\sin\phi\right)y\right].\end{aligned} \tag{A13}$$

$\bar{f}_{\rm RS}$ is expressed as

$$\begin{aligned}\bar{f}_{\rm RS} &= -\frac{1}{\beta}\lim_{n\to 0}\frac{1}{n}(\Phi_{\rm RS}+\Psi_{\rm RS})\\ &= -\frac{1}{\beta}\Bigg\{-(\hat{Q}_{\rm cc}Q_{\rm cc}+\hat{Q}_{\rm ss}Q_{\rm ss}+\hat{Q}_{\rm cs}Q_{\rm cs})+\frac{1}{2}(\hat{q}_{\rm cc}q_{\rm cc}+\hat{q}_{\rm ss}q_{\rm ss}+\hat{q}_{\rm cs}q_{\rm cs}+\hat{q}_{\rm sc}q_{\rm sc})\\ &\quad+\frac{\beta^2J^2}{4}\big(Q_{\rm cc}^2+Q_{\rm ss}^2+2Q_{\rm cs}^2-q_{\rm cc}^2-q_{\rm ss}^2-q_{\rm cs}^2-q_{\rm ss}^2\big),\\ &\quad+\int Dx\int Dy\log\int d\phi\exp\Bigg[\left(\hat{Q}_{\rm cc}-\frac{1}{2}\hat{q}_{\rm cc}\right)\cos^2\phi+\left(\hat{Q}_{\rm ss}-\frac{1}{2}\hat{q}_{\rm ss}\right)\sin^2\phi+\left(\hat{Q}_{\rm cs}-\frac{\hat{q}_{\rm cs}+\hat{q}_{\rm cs}}{2}\right)\sin\phi\cos\phi\\ &\quad+\sqrt{\frac{\hat{q}_{\rm cc}\hat{q}_{\rm ss}-\left(\frac{\hat{q}_{\rm cs}+\hat{q}_{\rm sc}}{2}\right)^2}{\hat{q}_{\rm ss}}}\cos\phi\,x+\left(\frac{\hat{q}_{\rm cs}+\hat{q}_{\rm sc}}{2\sqrt{\hat{q}_{\rm ss}}}\cos\phi+\sqrt{\hat{q}_{\rm ss}}\sin\phi\right)y\Bigg]\Bigg\}.\end{aligned}\tag{A14}$$

From the extrema conditions with respect to $q_{\rm cc}$, $q_{\rm ss}$, $q_{\rm cs}$, $q_{\rm sc}$ and $Q_{\rm cc}$, $Q_{\rm ss}$, $Q_{\rm cs}$, we obtain

$$\hat{q}_{\rm cc}=\beta^2J^2q_{\rm cc},\ \hat{q}_{\rm ss}=\beta^2J^2q_{\rm ss},\ \hat{q}_{\rm cs}=\beta^2J^2q_{\rm cs},\ \hat{q}_{\rm sc}=\beta^2J^2q_{\rm sc},\hat{Q}_{\rm cc}=\frac{\beta^2J^2}{2}Q_{\rm cc},\ \hat{Q}_{\rm ss}=\frac{\beta^2J^2}{2}Q_{\rm ss},\ \hat{Q}_{\rm cs}=\beta^2J^2Q_{\rm cs}.\tag{A15}$$

Thus, we have

$$\bar{f}_{\rm RS}=-\frac{1}{\beta}\left\{\frac{\beta^2J^2}{4}\big(q_{\rm cc}^2+q_{\rm ss}^2+q_{\rm cs}^2+q_{\rm sc}^2-Q_{\rm cc}^2-Q_{\rm ss}^2-2Q_{\rm cs}^2\big)+\int Dx\int Dy\log\int d\phi M(\phi|x,y)\right\},\tag{A16}$$

$$\begin{aligned}M(\phi|x,y)&=\exp\Bigg[\frac{\beta^2J^2}{2}(Q_{\rm cc}-q_{\rm cc})\cos^2\phi+\frac{\beta^2J^2}{2}(Q_{\rm ss}-q_{\rm ss})\sin^2\phi+\beta^2J^2\left(Q_{\rm cs}-\frac{q_{\rm cs}+q_{\rm sc}}{2}\right)\sin\phi\cos\phi\\ &\quad+\beta J\sqrt{\frac{q_{\rm cc}q_{\rm ss}-\left(\frac{q_{\rm cs}+q_{\rm sc}}{2}\right)^2}{q_{\rm ss}}}\cos\phi\,x+\beta J\left(\frac{q_{\rm cs}+q_{\rm sc}}{2\sqrt{q_{\rm ss}}}\cos\phi+\sqrt{q_{\rm ss}}\sin\phi\right)y\Bigg].\end{aligned}\tag{A17}$$

From this, we obtain the following SPEs:

$$Q_{\rm cc}=[\langle\cos^2\phi\rangle],\quad Q_{\rm ss}=[\langle\sin^2\phi\rangle]=1-Q_{\rm cc},\ Q_{\rm cs}=[\langle\sin\phi\cos\phi\rangle],\tag{A18}$$

$$q_{\rm cc}=[\langle\cos\phi\rangle^2],\quad q_{\rm ss}=[\langle\sin\phi\rangle^2],\ q_{\rm cs}=[\langle\sin\phi\rangle\langle\cos\phi\rangle]=q_{\rm sc},\tag{A19}$$

$$[\cdots]\equiv\int Dx\int Dy\cdots,\ \langle\cdots\rangle\equiv\frac{\int d\phi M(\phi|x,y)\ \cdots}{\int d\phi M(\phi|x,y)}.\tag{A20}$$

Using the above relations, $f_{\rm RS}$ and $M(\phi|x,y)$ are now expressed as

$$\bar{f}_{\rm RS}=-\frac{\beta J^2}{4}\big(q_{\rm cc}^2+q_{\rm ss}^2+2q_{\rm cs}^2-1+2Q_{\rm cc}(1-Q_{\rm cc})-2Q_{\rm cs}^2\big)-\frac{1}{\beta}\int Dx\int Dy\log\int d\phi M(\phi|x,y),\tag{A21}$$

$$\begin{aligned}M(\phi|x,y)&=\exp\Bigg[\frac{\beta^2J^2}{2}(Q_{\rm cc}-q_{\rm cc})\cos^2\phi+\frac{\beta^2J^2}{2}(1-Q_{\rm cc}-q_{\rm ss})\sin^2\phi+\beta^2J^2(Q_{\rm cs}-q_{\rm cs})\sin\phi\cos\phi\\ &\quad+\beta J\sqrt{\frac{q_{\rm cc}q_{\rm ss}-q_{\rm cs}^2}{q_{\rm ss}}}\cos\phi\,x+\beta J\left(\frac{q_{\rm cs}}{\sqrt{q_{\rm ss}}}\cos\phi+\sqrt{q_{\rm ss}}\sin\phi\right)y\Bigg].\end{aligned}\tag{A22}$$

As discussed in the main text, $Q_{\rm cc}=Q_{\rm ss}=\frac{1}{2}$, $Q_{\rm cs}=0$, $q_{\rm cc}=q_{\rm ss}$, and $q_{\rm cs}=0$ follow. Thus, we obtain

$$\bar{f}_{\rm RS}=-\frac{\beta J^2}{2}q_{\rm cc}^2-\frac{1}{\beta}\int Dx\int Dy\log\int d\phi M(\phi|x,y),\tag{A23}$$

$$M(\phi|x,y)=\exp\left[-\frac{\beta^2J^2}{2}q_{\rm cc}+\beta J\sqrt{q_{\rm cc}}(\cos\phi\,x+\sin\phi\,y)\right],\tag{A24}$$

where we omit irrelevant constants. Now, we introduce the polar coordinates, $x=r\cos\theta$, $y=r\sin\theta$. Then, we have

$$\bar{f}_{\rm RS}=-\frac{\beta J^2}{2}q_{\rm cc}^2-\frac{1}{\beta}\frac{1}{2\pi}\int_0^\infty dre^{-\frac{1}{2}r^2}r\int_0^{2\pi}d\theta\log\int d\phi M(\phi|r,\theta),\tag{A25}$$

$$M(\phi|r,\theta)=e^{-\frac{\beta^2J^2}{2}q_{\rm cc}+\beta J\sqrt{q_{\rm cc}}r\cos(\phi-\theta)}.\tag{A26}$$

By performing integration, we have

$$\bar{f}_{\mathrm{RS}} = -\frac{\beta J^2}{2} q_{\mathrm{cc}}^2 - \frac{1}{\beta}\int_0^\infty dr e^{-\frac{1}{2}r^2} r \log x \left[2\pi I_0(\beta J\sqrt{q_{\mathrm{cc}}}r) e^{-\frac{\beta^2 J^2}{2} q_{\mathrm{cc}}}\right]$$
$$= -\frac{\beta J^2}{2} q_{\mathrm{cc}}^2 + \frac{\beta J^2}{2} q_{\mathrm{cc}} - \frac{1}{\beta}\int_0^\infty dr e^{-\frac{1}{2}r^2} r \log[2\pi I_0(\beta J\sqrt{q_{\mathrm{cc}}}r)]. \tag{A27}$$

$I_n(x)$ is the nth order modified Bessel function of the first kind. The SPE becomes

$$-\beta J^2 q_{\mathrm{cc}} + \frac{\beta J^2}{2} - \frac{1}{\beta}\int_0^\infty dr e^{-\frac{1}{2}r^2} r \frac{I_1(\beta J\sqrt{q_{\mathrm{cc}}}r)}{I_0(\beta J\sqrt{q_{\mathrm{cc}}}r)} \beta J r \frac{1}{2\sqrt{q_{\mathrm{cc}}}} = 0. \tag{A28}$$

Since the spin glass order parameter is $q = 2q_{\mathrm{cc}}$, we obtain

$$q = 1 - \frac{k_{\mathrm{B}}T}{J}\sqrt{\frac{2}{q}}\int_0^\infty dr r^2 e^{-\frac{1}{2}r^2} \frac{I_1\left(\frac{J}{k_{\mathrm{B}}T}\sqrt{\frac{q}{2}}r\right)}{I_0\left(\frac{J}{k_{\mathrm{B}}T}\sqrt{\frac{q}{2}}r\right)}. \tag{A29}$$

This is nothing but the equation for q derived by Sherrington and Kirkpatrick [10].

[1] For example, see H. E. Stanley, in *Phase Transitions and Critical Phenomena*, edited by C. Domb and M. S. Green (Academic, London, 1974), Vol. 3, p. 486.

[2] D. S. Saunders, *An Introduction to Biological Rhythms* (Blackie, Glasgow, 1977).

[3] A. T. Cloudsley-Thompson, *Biological Clocks: Their Function in Nature* (Weidenfeld and Nicolson, London, 1980).

[4] A. T. Winfree, J. Theor. Biol. **16**, 15 (1967).

[5] Y. Kuramoto, in *Proceedings of the International Symposium on Mathematical Problems in Theoretical Physics*, edited by H. Araki (Springer, New York, 1975).

[6] Y. Kuramoto, *Chemical Oscillations, Waves, and Turbulence* (Springer-Verlag, Berlin, 1984).

[7] J. A. Acebrón, L. L. Bonilla, C. J. Pérez Vicente, and F. Ritort, Rev. Mod. Phys. **77**, 137 (2005), and papers cited therein.

[8] T. Uezu, T. Kimoto, S. Kiyokawa, and M. Okada, J. Phys. Soc. Jpn. **84**, 033001 (2015).

[9] T. Uezu (unpublished).

[10] D. Sherrington and S. Kirkpatrick, Phys. Rev. Lett. **35**, 1792 (1975).

[11] H. Daido, Phys. Rev. Lett. **68**, 1073 (1992).

[12] J. P. L. Hatchett and T. Uezu, Phys. Rev. E **78**, 036106 (2008).